Journal of Sound and Vibration (1998) **212**(3), 417–434

VIBRATION OF MULTI-SPAN TIMOSHENKO FRAMES DUE TO MOVING LOADS

R.-T. WANG AND J.-S. LIN

Department of Engineering Science, National Cheng Kung University, Tainan, Taiwan, Republic of China

(*Received* 8 *July* 1997, *and in final form* 23 *October* 1997)

An analytical method is presented in this paper to study the vibration of multi-span Timoshenko frames. The combined effects of axial inertia, rotatory inertia and shear deformation of each branch of those frames are simultaneously considered. Any two distinct sets of the mode shape functions are shown to be orthogonal. The method of modal analysis is then adopted to investigate the forced vibration of the frames. A concentrated load and a uniformly distributed load moving on these frames are treated as two examples. Results show that as the span number gets larger, the first modal frequency gets smaller. Furthermore, the longer column implies a smaller first modal frequency. The absolute maximum deflection of the Timoshenko frame is larger than that of the Bernoulli–Euler frame.

1. INTRODUCTION

Traditionally, the Bernoulli–Euler beam theory has been applied to analyse the dynamics of frameworks [1, 2]. The beam theory leads to erroneous results for cases of a large ratio of radius of gyration of cross-section to length and high modes [3]. The errors can be corrected by including the effects of rotatory inertia and shear deformation of beams [4]. Without including the effect of axial inertia, the Timoshenko beam theory has been extended to determine the modal frequencies of frames [5–7]. However, neglecting the effect cannot maintain structures such as T-type frames in equilibrium. Therefore, the effects of axial inertia, rotatory inertia and shear deformation of beams must be simultaneously included in studying the dynamics of frame structures.

The response of a multi-span frame to moving loads is a function of both time and spatial co-ordinates. The maximum deflection induced by a moving load is greater than that induced by the load in a static situation [8]. Therefore, designing frame structures from the perspective of static loads is unreliable. Consequently, the problem of loads moving on frame structures should be investigated in structural dynamics. Two approaches often adopted by engineers to analyse the dynamic responses of structures are the finite element technique and the method of modal analysis. The extensive computational time and computer memory storage requirements make the finite element technique impractical. It is suggested that the modal analysis methodology for analysing the vibration of multi-span Timoshenko frames be investigated.

In this paper, a multi-span Timoshenko frame is used as a model. All branches of the frame are homogeneous and isotropic with density ρ, Young's modulus E, shear modulus. G, Poisson's ratio μ and shear coefficient κ. Each branch has the cross-sectional area A, the second moment I of the cross-section with respect to the neutral axis and the radius η of gyration of the cross-section. The length L is the same for all spans. Moreover, all

0022–460X/98/180417 + 18 $25.00/0/sv971437

columns of the frame also have equal length L^*. The effects of rotatory inertia, shear deformation and axial inertia of each branch of the frame are accounted for in this study. The frequency–response relation at both ends of any branch is obtained by an analytical method. The conditions of displacement continuity and force balance at any junction of two adjacent spans and one connected column are adopted to set up the transfer matrix of response. The transfer matrix method is then employed to determine the modal frequencies and their corresponding mode shape functions of the frame. The orthogonality of any two distinct sets of the mode shape functions is demonstrated to guarantee the practice of the method of modal analysis. A concentrated load and a uniformly distributed load moving on the frame are taken as two examples. The length ratio of one column to one span is defined as l_r. The velocity and the distributed length of loads on the responses of those frames are studied. The effects of l_r and the span number on the characteristics of responses are also investigated. The computed results are compared with those of a multi-span Bernoulli–Euler frame.

2. EQUATIONS OF MOTION

Figure 1 depicts a distributed load $f(x, t)$ on an n-span Timoshenko frame. The equations of motion of the ith span are

$$\frac{\partial n_i}{\partial x} = \rho A \frac{\partial^2 u_i}{\partial t^2}, \qquad \frac{\partial q_i}{\partial x} + f_i(x, t) = \rho A \frac{\partial^2 w_i}{\partial t^2}, \tag{1a, b}$$

$$q_i - \frac{\partial m_i}{\partial x} = \rho I \frac{\partial^2 \psi_i}{\partial t^2}, \tag{1c}$$

where

$$n_i = EA \frac{\partial u_i}{\partial x}, \qquad q_i = \kappa GA\left(\frac{\partial w_i}{\partial x} - \psi_i\right), \qquad m_i = -EI \frac{\partial \psi_i}{\partial x}, \tag{2}$$

in which u_i is the longitudinal displacement, w_i is the transverse displacement, ψ_i is the rotatory angle, n_i is the axial force, q_i is the transverse shear force, m_i is the bending moment, x is the co-ordinate of the neutral axis, t is time and $f_i(x, t)$ is the component of load on the span. The sign convention for displacements and applied forces at both ends of the span (see Figure 2) are

$$\{u_{ia} w_{ia} \psi_{ia} n_{ia} q_{ia} m_{ia}\} = \{u_i w_i \psi_i - n_i - q_i m_i\}|_{x = (i-1)L}, \tag{3a}$$

$$\{u_{ib} w_{ib} \psi_{ib} n_{ib} q_{ib} m_{ib}\} = \{u_i w_i \psi_i n_i q_i - m_i\}|_{x = iL}. \tag{3b}$$

The equations of motion of the ith column of the frame are

$$\frac{\partial n_i^*}{\partial x_i} = \rho A \frac{\partial^2 u_i^*}{\partial x_i^2}, \qquad \frac{\partial q_i^*}{\partial x_i} = \rho A \frac{\partial^2 w_i^*}{\partial t^2}, \tag{4a, b}$$

$$q_i^* - \frac{\partial m_i^*}{\partial x_i} = \rho I \frac{\partial^2 \psi_i^*}{\partial t^2}, \tag{4c}$$

where u_i^*, w_i^*, ψ_i^*, n_i^*, q_i^*, m_i^* and x_i are the longitudinal displacement, transverse displacement, rotatory angle, axial force, transverse shear force, bending moment and axial

co-ordinate of the column respectively. The sign convention of displacements and applied forces at both ends of the column (see Figure 3) is

$$\{u_{ia}^* w_{ia}^* \psi_{ia}^* n_{ia}^* q_{ia}^* m_{ia}^*\} = \{u_i^* w_i^* \psi_i^* - n_i^* - q_i^* m_i^*\}|_{x_i = 0}, \tag{5a}$$

$$\{u_{ib}^* w_{ib}^* \psi_{ib}^* n_{ib}^* q_{ib}^* m_{ib}^*\} = \{u_i^* w_i^* \psi_i^* n_i^* q_i^* - m_i^*\}|_{x_i = L^*}. \tag{5b}$$

The displacement conditions at the fixed ends of the entire frame are

$$u_{1a} = u_{nb} = 0, \qquad w_{1a} = w_{nb} = 0, \qquad \psi_{1a} = \psi_{nb} = 0, \tag{6a}$$

$$u_{ib}^* = 0; \quad w_{ib}^* = 0, \quad \psi_{ib}^* = 0, \qquad i = 1, 2, \ldots, n-1. \tag{6b}$$

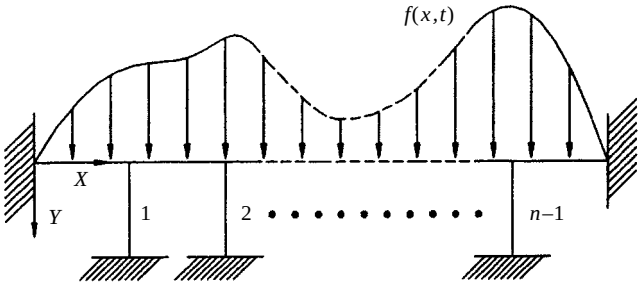

Figure 1. A distributed load $f(x, t)$ acts on an n-span Timoshenko frame.

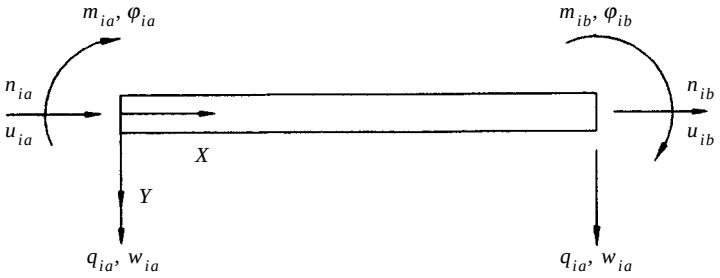

Figure 2. Applied end forces and displacements of the ith span.

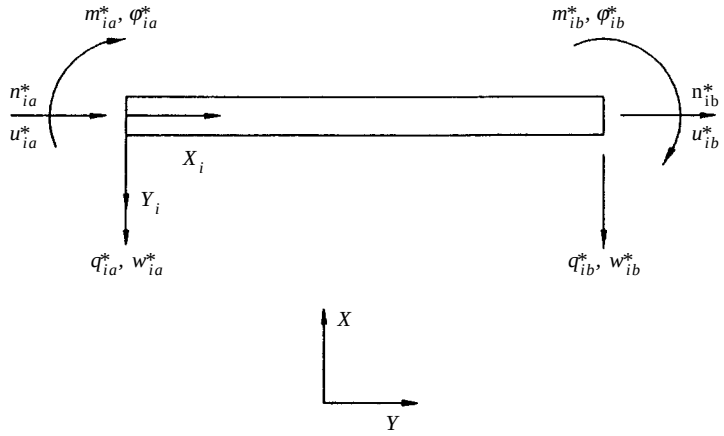

Figure 3. Applied end forces and displacements of the ith column.

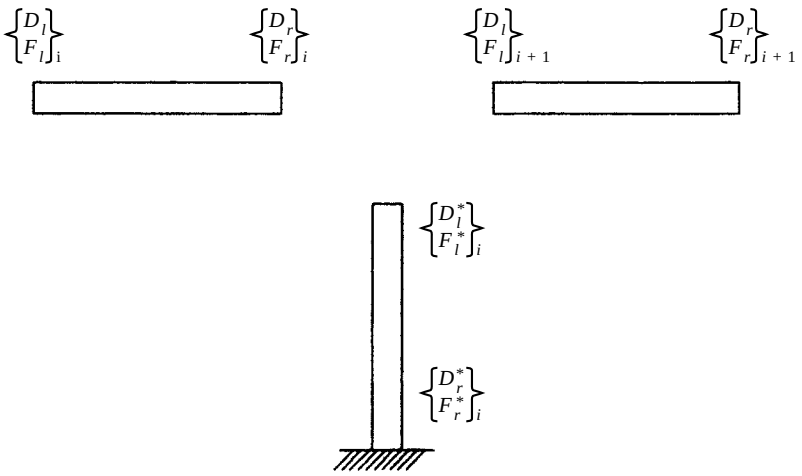

Figure 4. Applied end forces and displacements of a typical T-type frame.

The displacement continuity and the force balance at the ith junction of the ith column and two connected spans are

$$\psi_{ib} = \psi_{(i+1)a} = \psi_{ia}^*; \qquad u_{ib} = u_{(i+1)a} = -w_{ia}^*; \qquad w_{ib} = w_{(i+1)a} = u_{ia}^*, \tag{6c}$$

$$m_{ib} + m_{(i+1)a} + m_{ia}^* = 0, \qquad q_{ib} + q_{(i+1)a} + n_{ia}^* = 0, \qquad n_{ib} + n_{(i+1)a} - q_{ia}^* = 0. \tag{6d}$$

Equations (1)–(6d) constitute the equations of motion of the entire frame.

3. MODAL FREQUENCIES

To calculate the modal frequencies of the frame, the longitudinal displacement u_i, transverse deflection w_i, rotatory angle ψ_i, axial force n_i, transverse shear force q_i and bending moment m_i of the ith span can be expressed as

$$\{u_i w_i \psi_i n_i q_i m_i\}(x, t) = \{U_i W_i \Psi_i N_i Q_i M_i\}(x) \sin(\omega t), \tag{7}$$

in which ω is the circular frequency. The function $U_i(x)$ is [9]

$$U_i(x) = B_{1i} \cos(\lambda x) + B_{2i} \sin(\lambda x), \tag{8}$$

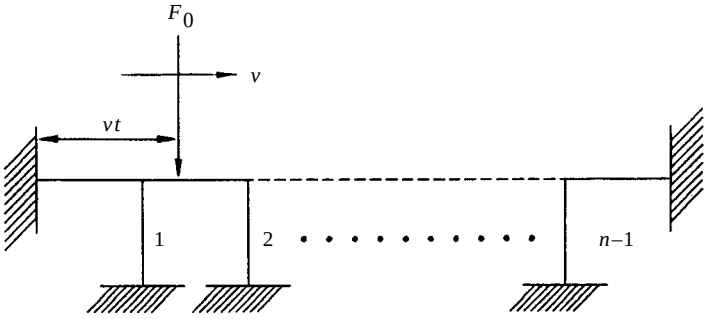

Figure 5. A concentrated force traversing on the n-span Timoshenko frame.

where $\lambda = (\rho/E)^{1/2}\omega$, and B_{1i} and B_{2i} are two constants. The functions $W_i(x)$ and $\Psi_i(x)$, respectively, are: case 1 for $\lambda^2 < \kappa/2(1+\mu)\eta^2$,

$$W_i(x) = B_{3i}\cosh(p_1 x) + B_{4i}\sinh(p_1 x) + B_{5i}\cos(p_2 x) + B_{6i}\sin(p_2 x), \tag{9a}$$

$$\Psi_i(x) = \beta_1(p_1)[B_{4i}\cosh(p_1 x) + B_{3i}\sinh(p_1 x)] + \beta_2(p_2)[B_{5i}\sin(p_2 x) - B_{6i}\cos(p_2 x)], \tag{9b}$$

where

$$p_1^2 = -\frac{\lambda^2}{2}\left[1 + \frac{2(1+\mu)}{\kappa}\right] + \left\{\frac{\lambda^4}{4}\left[1 + \frac{2(1+\mu)}{\kappa}\right]^2 + \left[\frac{\lambda^2}{\eta^2} - \frac{2(1+\mu)\lambda^4}{\kappa}\right]\right\}^{1/2},$$

$$p_2^2 = \frac{\lambda^2}{2}\left[1 + \frac{2(1+\mu)}{\kappa}\right] + \left\{\frac{\lambda^4}{4}\left[1 + \frac{2(1+\mu)}{\kappa}\right]^2 + \left[\frac{\lambda^2}{\eta^2} - \frac{2(1+\mu)\lambda^4}{\kappa}\right]\right\}^{1/2},$$

$$\beta_1(p) = \frac{1}{p}\left[p^2 + \frac{2(1+\mu)\lambda^2}{\kappa}\right], \qquad \beta_2(p) = \frac{1}{p}\left[-p^2 + \frac{2(1+\mu)\lambda^2}{\kappa}\right],$$

or case 2 for $\lambda^2 > \kappa/2(1+\mu)\eta^2$

$$W_i(x) = B_{3i}\cos(p_1 x) + B_{4i}\sin(p_1 x) + B_{5i}\cos(p_2 x) + B_{6i}\sin(p_2 x), \tag{9c}$$

$$\Psi_i(x) = \beta_2(p_1)[-B_{4i}\cos(p_1 x) + B_{3i}\sin(p_1 x)] + \beta_2(p_2)[B_{5i}\sin(p_2 x) - B_{6i}\cos(p_2 x)], \tag{9d}$$

where

$$p_1^2 = \frac{\lambda^2}{2}\left[1 + \frac{2(1+\mu)}{\kappa}\right] - \left\{\frac{\lambda^4}{4}\left[1 + \frac{2(1+\mu)}{\kappa}\right]^2 + \left[\frac{\lambda^2}{\eta^2} - \frac{2(1+\mu)\lambda^4}{\kappa}\right]\right\}^{1/2},$$

$$p_2^2 = \frac{\lambda^2}{2}\left[1 + \frac{2(1+\mu)}{\kappa}\right] + \left\{\frac{\lambda^4}{4}\left[1 + \frac{2(1+\mu)}{\kappa}\right]^2 + \left[\frac{\lambda^2}{\eta^2} - \frac{2(1+\mu)\lambda^4}{\kappa}\right]\right\}^{1/2},$$

$$\beta_2(p) = \frac{1}{p}\left[-p^2 + \frac{2(1+\mu)\lambda^2}{\kappa}\right].$$

Substituting equations (8)–(9d) into equation (2) yields the corresponding axial force $N_i(x)$, transverse shear force $Q_i(x)$ and bending moment $M_i(x)$. The constants B_{1i}–B_{6i} of equations (8)–(9d) are determined by boundary conditions of the ith span.

Similarly, the axial displacement, transverse deflection and rotatory angle of the ith column are

$$\{u_i^* w_i^* \psi_i^*\}(x_i, t) = \{U_i^* W_i^* \Psi_i^*\}(x_i)\sin(\omega t), \tag{10a}$$

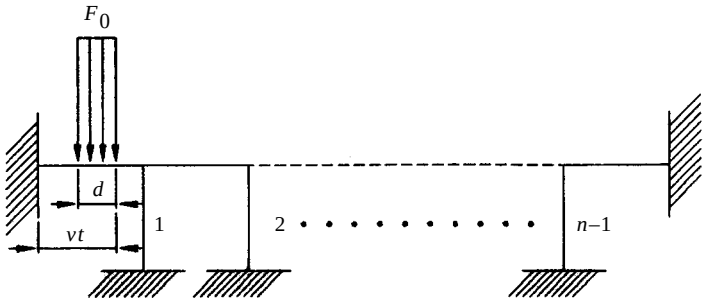

Figure 6. A uniformly distributed load traversing on the n-span Timoshenko frame.

which can be obtained by replacing the constants B_{1i}–B_{6i}, p_1, p_2, x and functions U_i, W_i, Ψ_i, β_1 and β_2 of equations (8)–(9d) with the constants B_{1i}^*–B_{6i}^*, p_1^*, p_2^*, x_i and functions U_i^*, W_i^*, Ψ_i^*, β_1^* and β_2^*. The corresponding axial force, transverse shear force and bending moment of the column are denoted as

$$\{n_i^* q_i^* m_i^*\}(x_i, t) = \{N_i^* Q_i^* M_i^*\}(x_i) \sin(\omega t). \tag{10b}$$

Substituting the functions $U_i(x)$, $W_i(x)$, $\Psi_i(x)$, $N_i(x)$, $Q_i(x)$ and $M_i(x)$ into equations (3a, b) and arranging the results into the symbolic vector forms, one obtains

$$\{U_{ia} W_{ia} \Psi_{ia} N_{ia} Q_{ia} M_{ia}\}^T = [P]_i \{B_{1i} B_{2i} B_{3i} B_{4i} B_{5i} B_{6i}\}^T, \tag{11a}$$

$$\{U_{ib} W_{ib} \Psi_{ib} N_{ib} Q_{ib} M_{ib}\}^T = [G]_i \{B_{1i} B_{2i} B_{3i} B_{4i} B_{5i} B_{6i}\}^T. \tag{11b}$$

The relation of displacements and forces at both ends of the ith span is therefore obtained to be of the form

$$\{U_{ib} W_{ib} \Psi_{ib} N_{ib} Q_{ib} M_{ib}\}^T = [R]_i \{U_{ia} W_{ia} \Psi_{ia} N_{ia} Q_{ia} M_{ia}\}^T, \tag{12}$$

where $[R]_i = [G]_i [P]_i^{-1}$. Similarly, the following relation

$$\{U_{ib}^* W_{ib}^* \Psi_{ib}^* N_{ib}^* Q_{ib}^* M_{ib}^*\}^T = [R^*]_i \{U_{ia}^* W_{ia}^* \Psi_{ia}^* N_{ia}^* Q_{ia}^* M_{ia}^*\}^T, \tag{13a}$$

is obtained for the ith column. Equation (13a) can be rearranged to the vector form

$$\{-W_{ib}^* U_{ib}^* \Psi_{ib}^* - Q_{ib}^* N_{ib}^* M_{ib}^*\}^T = [Z^*]_i \{-W_{ia}^* U_{ia}^* \Psi_{ia}^* - Q_{ia}^* N_{ia}^* M_{ia}^*\}^T. \tag{13b}$$

By introducing the following notations

$$\begin{aligned} \{D_l\}_j &= \{U_{ia} W_{ia} \Psi_{ia}\}^T, & \{D_r\}_i &= \{U_{ib} W_{ib} \Psi_{ib}\}^T, \\ \{F_l\}_i &= \{N_{ia} Q_{ia} M_{ia}\}^T, & \{F_r\}_i &= \{N_{ib} Q_{ib} M_{ib}\}^T, \end{aligned} \tag{14a}$$

$$\begin{aligned} \{D_l^*\}_i &= \{-W_{ia}^* U_{ia}^* \Psi_{ia}^*\}^T, & \{D_r^*\}_i &= \{-W_{ib}^* U_{ib}^* \Psi_{ib}^*\}^T, \\ \{F_l^*\}_i &= \{-Q_{ia}^* N_{ia}^* M_{ia}^*\}^T, & \{F_r^*\}_i &= \{-Q_{ib}^* N_{ib}^* M_{ib}^*\}^T, \end{aligned} \tag{14b}$$

equations (12) and (13b) are organized into the vector forms

$$\begin{Bmatrix} D_r \\ F_r \end{Bmatrix}_i = \begin{bmatrix} R_{11} & R_{12} \\ R_{21} & R_{22} \end{bmatrix}_i \begin{Bmatrix} D_l \\ F_l \end{Bmatrix}_i, \tag{15}$$

for the ith span and

$$\begin{Bmatrix} D_r^* \\ F_r^* \end{Bmatrix}_i = \begin{bmatrix} Z_{11}^* & Z_{12}^* \\ Z_{21}^* & Z_{22}^* \end{bmatrix}_i \begin{Bmatrix} D_l^* \\ F_l^* \end{Bmatrix}_i, \tag{16}$$

for the ith column respectively. Employing the condition of zero displacements at the fixed bottom of the ith column into equation (16) yields the relation of displacements and forces at the top of the column as

$$\{F_l^*\}_i = -[Z_{12}^{*-1} Z_{11}^*]_i \{D_l^*\}_i. \tag{17}$$

The conditions of the displacement continuity and the force balance

$$\{D_r\}_i = \{D_l\}_{i+1} = \{D_l^*\}_{i+1}, \tag{18a}$$

$$\{F_r\}_i + \{F_l\}_{i+1} + \{F_l^*\}_{i+1} = \{000\}^T, \tag{18b}$$

at the jth junction of two adjacent spans and the ith column of the frame (see Figure 4) imply that the relation of displacements and forces at the junction between the ith span and the $(i+1)$th span is

$$\begin{Bmatrix} D_l \\ F_l \end{Bmatrix}_{i+1} = \begin{bmatrix} I_{3\times 3} & 0 \\ Z_{12}^{*-1} Z_{11}^* & -I_{3\times 3} \end{bmatrix}_i \begin{Bmatrix} D_r \\ F_r \end{Bmatrix}_i, \tag{19}$$

where $I_{3\times 3}$ is an identity matrix of order 3. Therefore, the response relation at the left junction of the ith span and the $(i+1)$th span is

$$\begin{Bmatrix} D_l \\ F_l \end{Bmatrix}_{i+1} = [S]_i \begin{Bmatrix} D_l \\ F_l \end{Bmatrix}_i, \tag{20}$$

where the transfer matrix $[S]_i$ is

$$[S]_i = \begin{bmatrix} I_{3\times 3} & 0 \\ Z_{12}^{*-1} Z_{11}^* & -I_{3\times 3} \end{bmatrix}_i \begin{bmatrix} R_{11} & R_{12} \\ R_{21} & R_{22} \end{bmatrix}_i.$$

The jth modal frequency ω_j of the frame and the corresponding set of the mode shape functions $\{U_i^j, W_i^j, \Psi_i^j\}(x)$ of the ith span and $\{U_i^{*j}, W_i^{*j}, \Psi_i^{*j}\}(x_i)$ of the ith column are obtained by performing similar calculations described by Wang and Lin [10]. To simplify the notations in the following sections, the jth set of the mode shape functions and the corresponding set of axial force, transverse shear force and bending moment of the entire span of the frame are denoted, respectively, as $\{U^j, W^j, \Psi^j\}(x)$ and $\{N^j, Q^j, M^j\}(x)$ where $0 \leqslant x \leqslant nL$. Furthermore, the corresponding set of axial force, transverse shear force and bending moment of the ith column are indicated as $\{N_i^{*j}, Q_i^{*j}, M_i^{*j}\}$, respectively.

4. ORTHOGONALITY OF MODE SHAPE FUNCTIONS

By performing similar procedures as described by Wang and Lin [10], the two following equations are obtained

$$\int_0^{nL} (\rho A U^j U^k + \rho A W^j W^k + \rho I \Psi^j \Psi^k)\, \mathrm{d}x + \sum_{j=1}^{n-1} \int_0^{L^*} (\rho A U_i^{*j} U_i^{*k} + \rho A W_i^{*j} W_i^{*k} + \rho I \Psi_i^{*j} \Psi_i^{*k})\, \mathrm{d}x_i = 0, \qquad j \neq k, \tag{21}$$

$$\int_0^{nL} \left(U^j \frac{\mathrm{d}N^k}{\mathrm{d}x} + W^j \frac{\mathrm{d}Q^k}{\mathrm{d}x} + \Psi^j \left(Q^k - \frac{\mathrm{d}M^k}{\mathrm{d}x} \right) \right) \mathrm{d}x + \sum_{j=1}^{n-1} \int_0^{L^*} \left(U_i^{*j} \frac{\mathrm{d}N_i^{*k}}{\mathrm{d}x_i} + W_i^{*j} \frac{\mathrm{d}Q_i^{*k}}{\mathrm{d}x_i} + \Psi_i^{*j} \left(Q_i^{*k} - \frac{\mathrm{d}M_i^{*k}}{\mathrm{d}x_i} \right) \right) \mathrm{d}x_i = 0, \qquad j \neq k. \tag{22}$$

It can be seen that two distinct modal frequencies and their corresponding sets of the mode shape functions are orthogonal.

5. FORCED VIBRATION

According to the orthogonality of two distinct sets of the mode shape functions, the superposition method is adopted in this section to study the forced vibration of the frame. The respective longitudinal displacement, transverse deflection, rotatory angle, axial force, transverse shear force and bending moment of the entire span are

$$\{uw\psi nqm\}(x, t) = \sum_{j=1} a_j(t) \{U^j W^j \Psi^j N^j Q^j M^j\}(x). \tag{23a}$$

The longitudinal displacement, transverse deflection, rotatory angle, axial force, transverse shear force and bending moment of the ith column, respectively, are

$$\{u_i^* w_i^* \psi_i^* n_i^* q_i^* m_i^*\}(x_i, t) = \sum_{j=1} a_j(t) \{U_i^{*j} W_i^{*j} \Psi_i^{*j} N_i^{*j} Q_i^{*j} M_i^{*j}\}(x_i). \tag{23b}$$

TABLE 1

The span number effect on the comparison of the first modal frequency $\bar{\omega}_1$ of two kinds of multi-span frames ($r = 0{\cdot}03$, $l_r = 1$)

Span	Timoshenko frame	Bernoulli–Euler frame
2	43·85	46·14
3	38·64	40·28
4	36·67	38·09
5	35·73	37·09
6	35·22	36·50
7	34·91	36·15

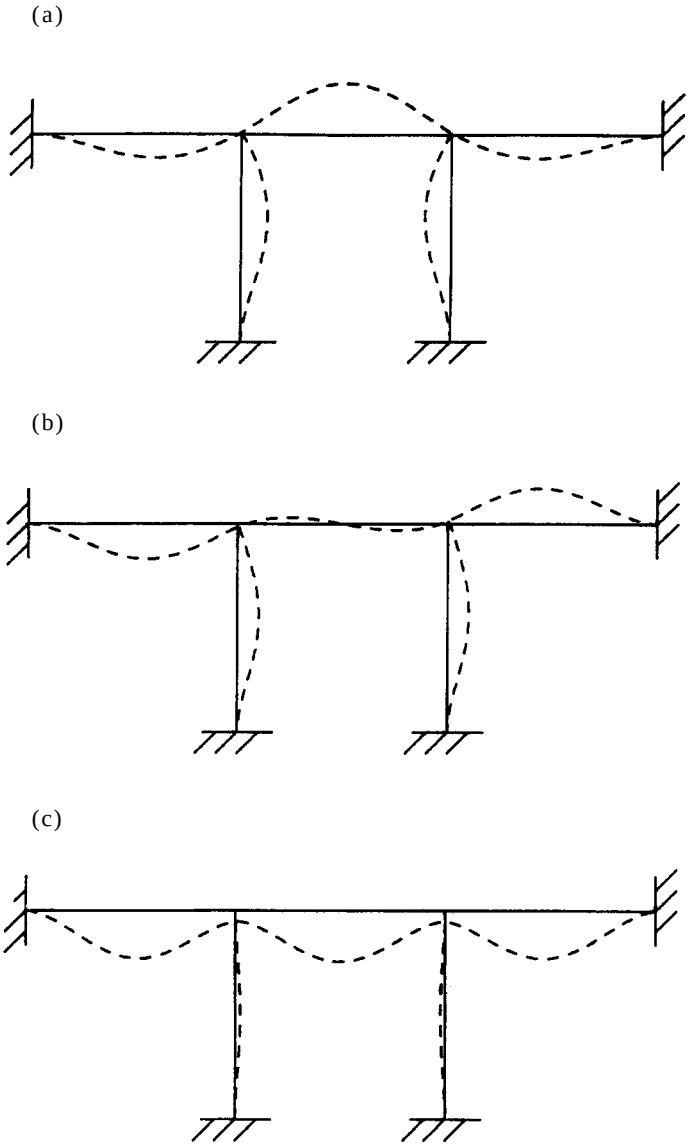

Figure 7. The lowest three modal frequencies and their corresponding mode shapes of a three-span Timoshenko frame ($r = 0{\cdot}03$, $l_r = 1$): (a) the first mode, $\bar{\omega}_1 = 38{\cdot}64$; (b) the second mode, $\bar{\omega}_2 = 47{\cdot}87$; and (c) the third mode, $\bar{\omega}_3 = 55{\cdot}61$.

By performing similar procedures to those described by Wang and Lin [10], the governing equation of the kth modal amplitude a_k is obtained as

$$\frac{\mathrm{d}^2 a_k}{\mathrm{d}t^2} + \omega_k^2 a_k = g_k(t), \tag{24}$$

in which ω_k is the kth modal frequency and the corresponding excitation $g_k(t)$ is

$$g_k(t) = \int_0^{nL} f(x, t) W^k(x)\, \mathrm{d}x / \xi_k, \tag{25}$$

where the modal mass ξ_k is

$$\xi_k = \int_0^{nl} (\rho A U^k U^k + \rho A W^k W^k + \rho I \Psi^k \Psi^k)\, \mathrm{d}x$$

$$+ \sum_{i=1}^{n-1} \int_0^{L^*} (\rho A U_i^{*k} U_i^{*k} + \rho A W_i^{*k} W_i^{*k} + \rho I \Psi_i^{*k} \Psi_{-i}^{*k})\, \mathrm{d}x_i, \tag{26}$$

6. MOVING LOADS

In this section, two types of moving loads are considered: concentrated load and uniformly distributed load [10].

6.1. CONCENTRATED LOAD

Figure 5 depicts a concentrated load of magnitude F_0 travelling at a constant velocity v on the multi-span frame. The load's form is expressed as

$$f(x, t) = F_0 \delta(x - vt), \tag{27}$$

where δ is the impulse function.

6.2. UNIFORMLY DISTRIBUTED LOAD

Figure 6 depicts a uniformly distributed load of magnitude f_0 travelling on the multi-span frame at a constant velocity v. The load's form is

$$f(x, t) = f_0[H(x + d - vt) - H(x - vt)], \tag{28}$$

where H is the unit step function and d is the distributed length.

7. EXAMPLES

To illustrate the numerical results in this study, the non-dimensional variables are introduced as

$$(\bar{u}, \overline{u_i^*}) = (u, u_i^*)/L, \qquad (\bar{w}, \overline{w_i^*}) = (w, w_i^*)/\eta, \qquad (\bar{\psi}, \overline{\psi_i^*}) = (\psi, \psi_i^*)L/\eta,$$

$$(\bar{x}, \overline{x_i}) = (x, x_i)/L, \qquad (\bar{n}, \overline{n_i^*}) = (n, n_i^*)/EA, \qquad (\bar{q}, \overline{q_i^*}) = (q, q_i^*)L^3/EI\eta,$$

$$(\bar{m}, \overline{m_i^*}) = (m, m_i^*)L^2/EI\eta, \qquad r = \eta/L, \qquad \bar{v} = v(\rho/E)^{1/2}/r, \qquad \epsilon = E/\kappa G, \qquad \overline{d} = d/L,$$

$$\overline{F}_0 = F_0 L^3/EI\eta, \qquad \overline{f}_0 = f_0 L^4/EI\eta, \qquad (\overline{t}, \overline{T}) = (EI/\rho A L^4)^{1/2}(t, L/v), \qquad l_r = L^*/L,$$

where l_r is the ratio of the length of a column to that of one span. Moreover, the shear coefficient $\kappa = 2/3$, Poisson's ratio $\mu = 1/3$ and $r = 0{\cdot}03$ of each branch are taken for the purpose of numerical analysis in this section. The initial conditions are set to be zero. Both values of $\overline{F}_0$ and $\overline{f}_0\overline{d}$ are assumed to be unity.

The following parameters are defined to illustrate the numerical results: non-dimensional frequency, $\bar{\omega}(=100\omega(\rho/E)^{1/2}L)$; maximum deflection of the beams during the motion of load, $\overline{W}_{max}$; the location of $\overline{W}_{max}$ appears, $\overline{X}_w$; loading time at which $\overline{W}_{max}$ appears, $\overline{T}_w$; maximum moment of the beams during the motion of load, $\overline{M}_{max}$; the location of $\overline{M}_{max}$ appears, $\overline{X}_M$; loading time at which $\overline{M}_{max}$ appears, $\overline{T}_M$; velocity ratio, $\alpha(=100v(\rho/E)^{1/2})$; the absolute maximum deflection $\overline{W}_g$; the critical velocity at which $\overline{W}_g$ appears, v_c; the velocity ratio at which $\overline{W}_g$ appears, α_w; the velocity ratio at which the absolute maximum moment appears, α_M; the ratio of the critical velocity to the lowest bending wave velocity, $\alpha_c(=v_c\pi/\omega_1 L)$.

Table 1 shows that the first modal frequency of the Timoshenko frame is always less than that of the Bernoulli–Euler frame. Furthermore, the results listed in this table also indicate that the deviation of the first modal frequency between these two frames becomes less as the span number increases. The lowest three modal frequencies and their corresponding mode shapes of a three-span Timoshenko frame ($l_r = 1$) are displayed in Figures 7(a–c), respectively. The first mode of the frame is a bending mode. Results obtained by the method of modal analysis converge rather fast. Therefore, it is sufficient to employ the lowest 16 modal frequencies and their corresponding sets of mode shape functions of multi-span frames in the method of modal analysis in the numerical computation. Note that the velocity range considered in this section is $0 \leqslant \alpha \leqslant 16$.

The comparisons of two different α effects on both histories of the deflection and the moment at the mid-point of the second span of a three-span Timoshenko frame ($l_r = 1$) induced by a concentrated moving load are displayed in Figures 8(a) and (b), respectively. A faster speed of the moving load results in a shorter duration of forced vibration of the frame. Consequently, those figures reveal that a large deflection and a large moment induced by a subcritical moving load ($\alpha = 2$) appear when the load travels on the frame.

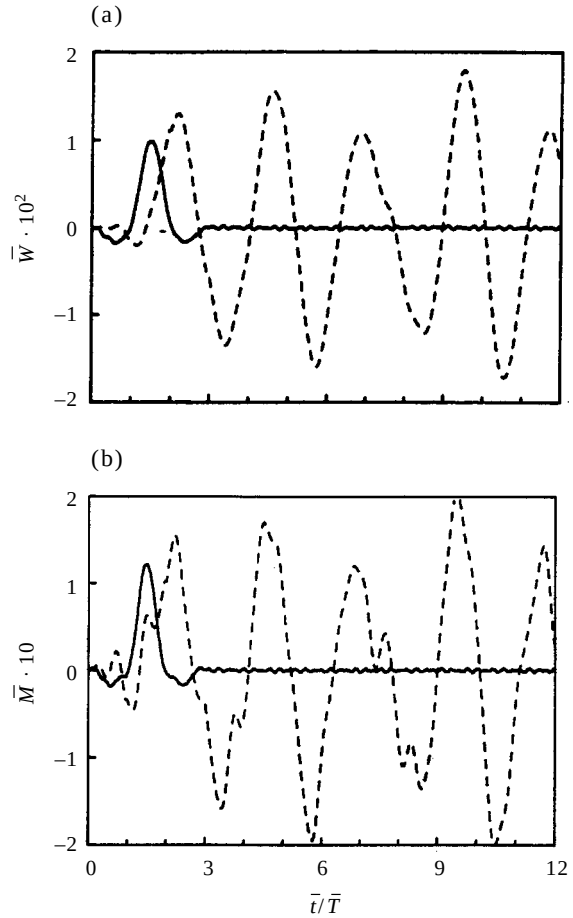

Figure 8. Comparisons of two α effects of a moving concentrated load on: (a) the deflection history; (b) the moment history of the mid-point of the second span of a three-span Timoshenko frame ($r = 0{\cdot}03$, $l_r = 1$). ——, $\alpha = 2$; ——, $\alpha = 15$.

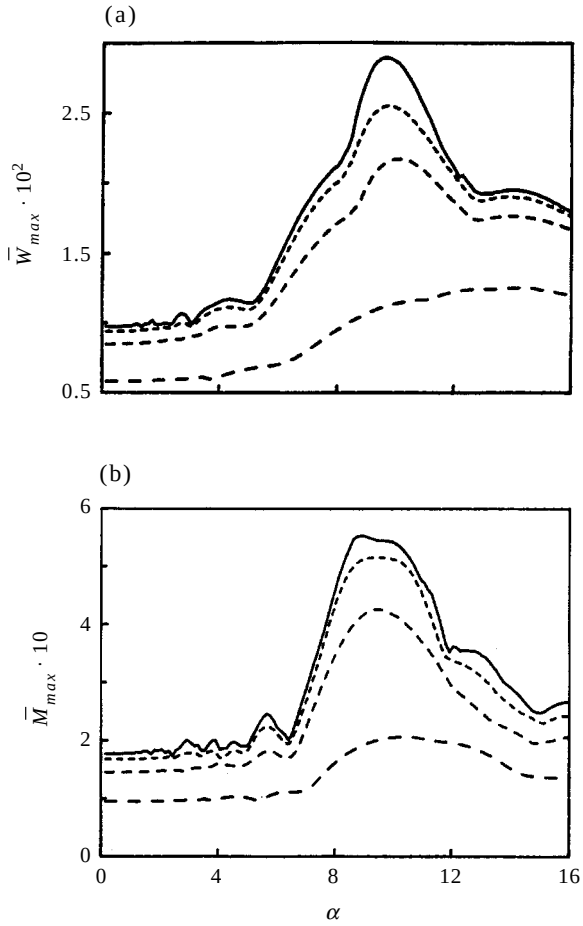

Figure 9. Comparisons of distributed loads on: (a) $\bar{W}_{max} - \alpha$, and (b) $\bar{M}_{max} - \alpha$ distributions of a three-span Timoshenko frame ($r = 0{\cdot}03$, $l_r = 1$). ——, Concentrated; ----, $\bar{d}=0{\cdot}25$; ——, $\bar{d} = 0{\cdot}5$; — — —, $\bar{d} = 1$.

Moreover, in Figures 8(a) and (b) it is shown that a large deflection and a large moment induced by a supercritical moving load ($\alpha = 15$) will appear after the load has left the frame.

The comparisons of the four different effects of distributed length $\bar{d}$ of load on the $\bar{W}_{max} - \alpha$ and $\bar{M}_{max} - \alpha$ distributions of a three-span Timoshenko frame ($l_r = 1$) are displayed in Figures 9(a) and (b), respectively. According to those figures, the more narrowly distributed length of load implies a larger deflection and a larger moment of the frame. Furthermore, a narrower load implies a more apparent α_w and α_M of the frame, as indicated in Figures 9(a) and (b), respectively. According to these findings, only the effects of a concentrated moving load on the responses of multi-span frames are considered in the following discussions.

The $\bar{W}_{max} - \alpha$ distribution displayed in Figure 10(a) indicates that the maximum deflection of a three-span Timoshenko frame is greater than that of a Bernoulli–Euler frame within the velocity range $0 \leqslant \alpha \leqslant 8$. The first modal frequency of the structure dominates the frame's vibration. Therefore, the bending wave is the dominant factor on

the vibration of the frame. Consequently, the value of α_w of the Timoshenko frame is less than that of the Bernoulli–Euler frame. The $\bar{X}_w - \alpha$ distribution displayed in Figure 10(b) reveals that the maximum deflection always appears near the mid-point of the second span except for $\alpha = 8$. The $\bar{T}_w - \alpha$ displayed in Figure 10(c) indicates that the maximum deflection induced by a subcritical moving load occurs when the load travels on the frame. Moreover, results of this figure also reveal that the maximum deflection induced by a supercritical moving load will appear after the load has left the frame.

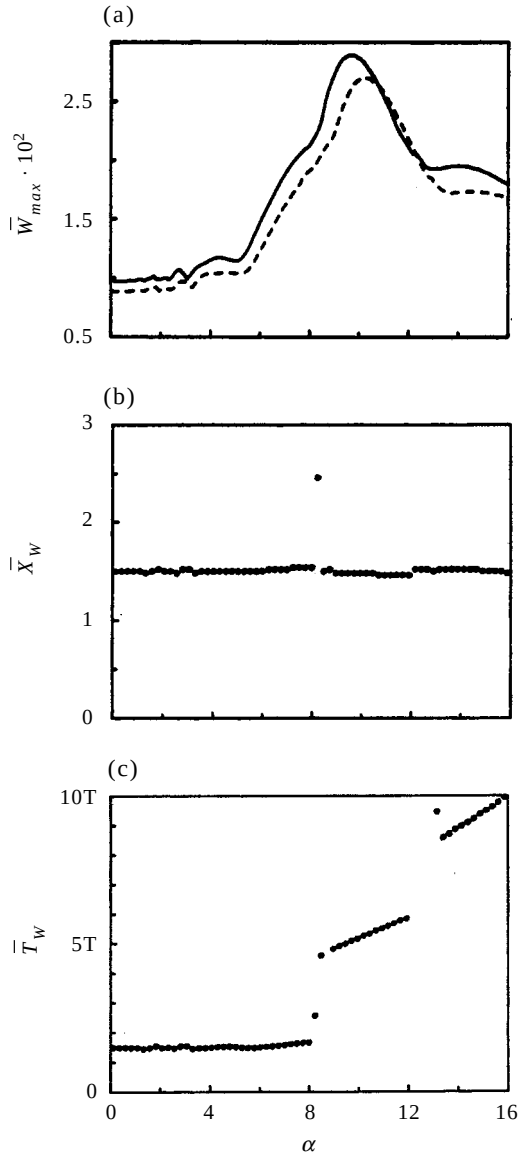

Figure 10. (a) The $\bar{W}_{max} - \alpha$ distribution (——, Timoshenko frame; – – –, Bernoulli–Euler frame) and its corresponding (b) $\bar{X}_w - \alpha$ and (c) $\bar{T}_w - \alpha$ distributions of a three-span Timoshenko frame ($r = 0{\cdot}03$, $l_r = 1$) due to a moving concentrated load.

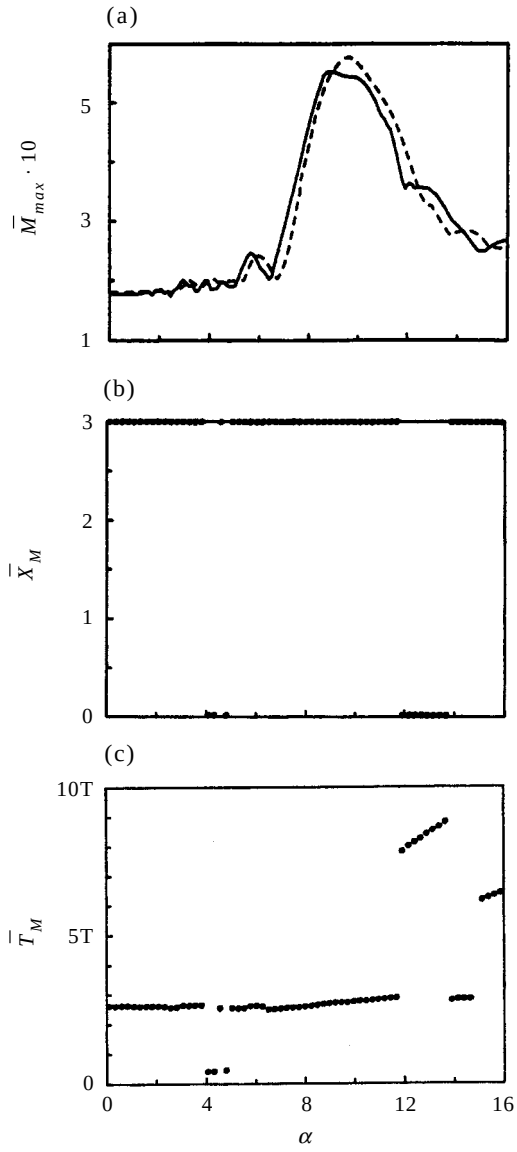

Figure 11. (a) The $\bar{M}_{max} - \alpha$ distribution (——, Timoshenko frame; – – –, Bernoulli–Euler frame) and its corresponding (b) $\bar{X}_m - \alpha$ and (c) $\bar{T}_m - \alpha$ distributions of a three-span Timoshenko frame ($r = 0{\cdot}03$, $l_r = 1$) due to a moving concentrated load.

The $\bar{M}_{max} - \alpha$ distribution displayed in Figure 11(a) shows that the maximum moment of a three-span Bernoulli–Euler frame is slightly larger than that of a three-span Timoshenko frame within the low velocity range $0 \leqslant \alpha \leqslant 4$. The effects of rotatory inertia and shearing deformation cause the maximum moment of the Timoshenko frame to be larger than that of the Bernoulli–Euler frame within the velocity range $7 \leqslant \alpha \leqslant 8$. The $\bar{X}_M - \alpha$ distribution displayed in Figure 11(b) reveals that the maximum moment always

TABLE 2

Both effects of the value of ratio l_r and span number on the first modal frequency $\bar{\omega}_1$ of a multi-span Timoshenko frame ($r = 0{\cdot}03$)

Span	$l_r = 0{\cdot}5$	$l_r = 1{\cdot}0$	$l_r = 1{\cdot}2$
2	50·17	43·85	36·13
3	45·09	38·64	33·30
4	43·20	36·67	31·95
5	42·30	35·73	31·26
6	41·81	35·22	30·87
7	41·51	34·91	30·64

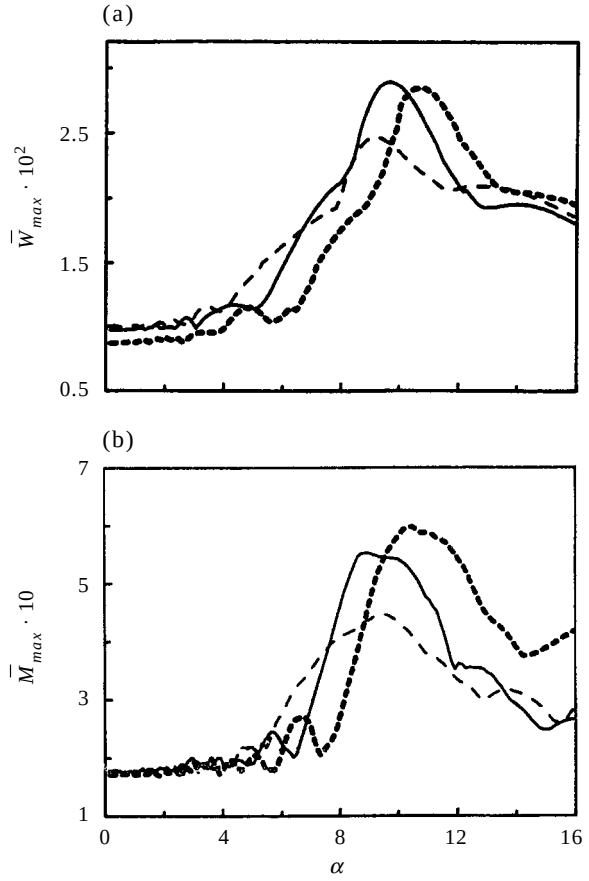

Figure 12. Comparisons of three l_r values on: (a) $\bar{W}_{max} - \alpha$, and (b) $\bar{M}_{max} - \alpha$ distributions of a three-span Timoshenko frame ($r = 0{\cdot}03$) due to a moving concentrated load. ——, $l_r = 1$; ----, $l_r = 0{\cdot}5$; ——, $l_r = 1{\cdot}2$.

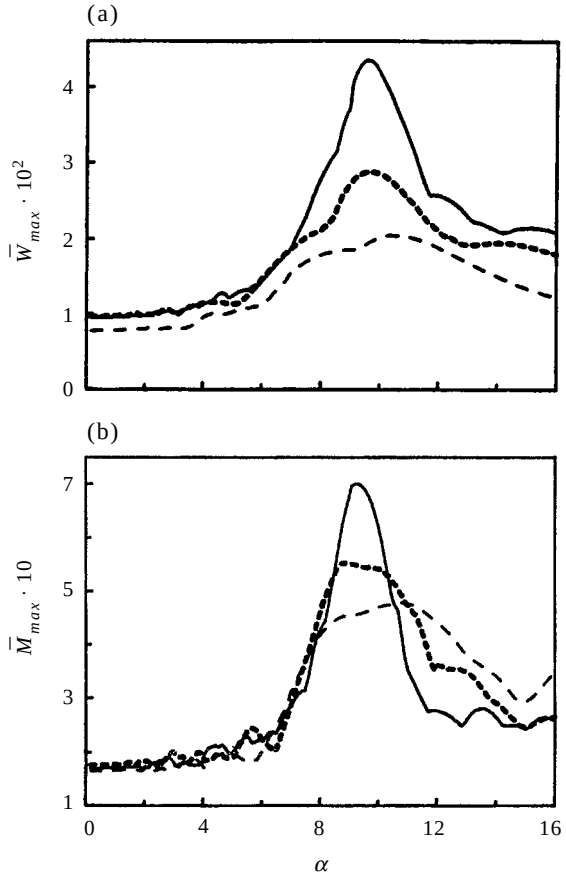

Figure 13. Span number effect on: (a) $\bar{W}_{max} - \alpha$, and (b) $\bar{M}_{max} - \alpha$ distributions of a multi-span Timoshenko frame ($r = 0{\cdot}03$, $l_r = 1$) due to a moving concentrated load. ——, 5 spans; ----, 3 spans; – – –, 2 spans.

appears at one fixed end of the frame. The $\bar{T}_M - \alpha$ distribution displayed in Figure 11(c) indicates that the maximum moment induced by a moving load ($\alpha \leqslant 12$) occurs when the load travels on the frame.

Table 2 compares the effects of three different values of l_r ($=0{\cdot}5$, 1, $1{\cdot}2$) on the first modal frequency of a multi-span frame. In Table 2 it is shown that the shorter column length causes a greater $\bar{\omega}_1$. A shorter column and a greater $\bar{\omega}_1$ imply that a shorter column induces a stiffer frame. The comparisons of three different l_r on the $\bar{W}_{max} - \alpha$ and $\bar{M}_{max} - \alpha$ distributions of a three-span Timoshenko frame ($r = 0{\cdot}03$) are displayed in Figures 12(a) and (b), respectively. Within the low velocity range of $0 \leqslant \alpha \leqslant 4$, the moving load can be regarded as a quasi-static load. Consequently, a shorter column implies a smaller value of $\bar{W}_{max}$ within the velocity range, as indicated in Figure 12(a). However, those three l_r effects on the deviation of the $\bar{M}_{max} - \alpha$ distributions are not obvious within the velocity range, as indicated in Figure 12(b). A higher first modal frequency implies a higher velocity of the bending wave. Therefore, both Figures 12(a) and (b) reveal that a shorter column implies both higher values of α_w and α_M.

The effect of span number on the $\bar{W}_{max} - \alpha$ distribution and the $\bar{M}_{max} - \alpha$ distribution of a multi-span Timoshenko frame ($l_r = 1$) are displayed in Figures 13(a) and (b), respectively. A travelling load induces a disturbance propagation in the frame. The

TABLE 3

The span number effect on the α_c ($=v_c\pi/\omega_1 L$) value and the absolute maximum deflection W_g of a multi-span frame ($r = 0{\cdot}03$, $l_r = 1$)

	Timoshenko frame		Bernoulli–Euler frame	
Span	$100W_g$	α_c	$100W_g$	α_c
2	2·05	0·75	1·81	0·75
3	2·89	0·79	2·70	0·80
4	3·54	0·83	3·39	0·83
5	4·35	0·84	4·08	0·85
6	5·05	0·85	4·83	0·86
7	5·64	0·85	5·50	0·86

composition of the disturbance contains free waves and non-propagating parts, which decay spatially. Under this circumstance, the effects of free waves on the vibration of the frame are more apparent for higher span numbers. Consequently, both figures indicate that the higher the number of the span, the more $\bar{W}_{max}$ and $\bar{M}_{max}$ are constrained within the neighbourhood of α_w and α_M, respectively. Table 3 shows that the larger span number of the frame ($l_r = 1$) has both greater values of α_c and $\bar{W}_g$. Furthermore, the absolute maximum deflection of the Timoshenko frame is greater than that of the Bernoulli–Euler frame. Results listed in this table also indicate that the lowest bending wave velocity is the upper bound of the critical velocity of the multi-span frame. Moreover, the effect of the bending wave on the vibration of the frame is more apparent for a high span number.

8. CONCLUSIONS

Based on the present modal analysis for the vibration of multi-span Timoshenko frames, the following conclusions can be made: (1) both maximum deflection and moment of a multi-span Timoshenko frame caused by a constant-velocity moving load are greater than those by the same static load; (2) a critical velocity exists at which the displacement of the frame becomes absolutely large; (3) both a large deflection and a large moment of a frame induced by a load moving with a subcritical velocity occur while the load travels on the frame; (4) a load moving with a supercritical velocity causes the maximum deflection of the frame to appear after the load has left the frame; (5) a shorter column implies a higher critical velocity; (6) the lowest bending wave velocity in the multi-span frame is the upper bound of the critical velocity of the frame; (7) the maximum moment always occurs at one fixed end of the entire beam; (8) the maximum deflection always occurs near the centre of the middle span of the entire beam; (9) the first modal frequency of a multi-span Timoshenko frame is less than that of a Bernoulli–Euler frame; and (10) the absolute maximum deflection of a multi-span Timoshenko frame is greater than that of a Bernoulli–Euler frame.

ACKNOWLEDGMENT

The authors would like to thank the National Science Council, R.O.C. for financial support of this manuscript under Contract No. 85-2212-E006-112.

REFERENCES

1. M. F. Rubinstein and W. C. Hurty 1961 *Journal of the Engineering Mechanics Division*, *American Society of Civil Engineers* **87**, 135–157. Effect of joint rotation on dynamics of structures.
2. K. W. Levien and B. J. Hartz 1963 *Journal of the Structural Division*, *American Society of Civil Engineers* **89**, 515–536. Dynamic flexibility matrix analysis of frames.
3. R. W. Clough 1955 *Bulletin of the Seismological Society of America* **45**, 289–301. On the importance of higher modes of vibration in the earthquake response of a tall building.
4. S. P. Timoshenko 1921 *Philosophical Magazine* **42**, 744–746. On the correction for shear of the differential equation for transverse vibrations of prismatic bars.
5. F. Y. Cheng 1970 *Journal of the Structural Division*, *American Society of Civil Engineers* **96**, 551–571. Vibrations of Timoshenko beams and frameworks.
6. G. B. Warburton and R. D. Henshell 1969 *International Journal for Numerical Methods in Engineering* **1**, 47–66. Transmission of vibration in beam systems.
7. T. M. Wang and T. A. Kinsman 1971 *Journal of Sound and Vibration* **14**, 215–227. Vibrations of frame structures according to the Timoshenko theory.
8. R. T. Wang and S. F. Lee 1993 *Journal of Civil and Hydraulic Engineering* (ROC) **20**, 7–18. Dynamic analysis of multispan frames subjected to moving loads using the finite element method.
9. R. T. Wang and J. S. Lin 1998 *Structural Engineering and Mechanics*, *An International Journal* (in press). Vibration of T-type Timoshenko frames subjected to moving loads.
10. R. T. Wang and J. S. Lin 1997 *Journal of the Chinese Society of Mechanical Engineers* **18**, 151–162. Vibration of multispan frames to moving loads.